Computation of Low-Speed Flow with Heat Addition

Charles L. Merkle* and Yun-Ho Choi†
The Pennsylvania State University, University Park, Pennsylvania

A perturbation expansion is used to obtain a system of conservation laws for compressible flows that is valid at arbitrarily low Mach numbers. These equations are rendered hyperbolic by adding an artificial time derivative to the energy equation, thus introducing pseudoacoustic waves with a speed the same order as the particle velocity. Traditional time-iterative schemes are shown to be effective in solving this system numerically. Stability calculations of the complete vector system indicate unconditional stability at all Mach numbers in the absence of gravity, but the source term introduced by buoyancy becomes destabilizing at Froude numbers below about 1. This instability is amplified by approximate factorization thus precluding solutions with gravity below this Mach number level. Computations of strong heat addition in low-Mach-number flow both with and without gravity confirm the stability predictions. Convergent solutions are maintained and are used to show the effect of gravity on such flowfields.

Introduction

THE computation of low-Mach-number flows has continued to be a challenge to contemporary compressible flow algorithms. Low-Mach-number applications of interest include both low-speed regions in an otherwise high-speed flow, and flows in which the velocity is slow throughout, but where heat addition causes compressibility effects to be significant. Although combustion problems are representative of the latter, the present authors' interest is in conjunction with the absorption of laser energy in a flowing gas.[1-4] The examples used in the present paper are for a derivative of the laser heating problem, namely, specified volumetric heat addition in a flowing gas, but the primary focus of the paper is on the general issue of the convergence characteristics of contemporary time-marching algorithms in low-Mach-number flows. The problems considered are two-dimensional and attention is limited to steady-state, inviscid solutions. Extension to three-dimensional geometries requires no new developments. Because low-velocity flows with heat addition can be affected by buoyancy, the effects of gravity are also addressed.

It is well known that time-dependent schemes become ineffective at low Mach numbers. Several recent papers[5-7] have addressed this problem and have identified distinct, but related, methods for circumventing it. Briley et al.[5] have used a rescaling of the equations to improve convergence at lower Mach numbers. The only calculation they reported was for a Mach number of 0.05, but their rescaling gave reasonable convergence for this single case. Turkel[6] developed a matrix preconditioning procedure for explicit schemes, but did not present any numerical results. The present authors independently developed a similar preconditioning scheme for implicit algorithms.[7] Our results showed that with preconditioning, identical rates of convergence could be obtained for Mach numbers from 0.7 down to 0.05.

Despite these improvements in low-Mach-number capability, these schemes are not adequate below Mach numbers of about 0.01. In the laser absorption problem mentioned above, Mach numbers as low as 10^{-4} are of interest. Similar Mach numbers are also encountered in laminar flame problems which are of considerable interest for scientific, if not for practical, reasons. Also, improved understanding of the convergence of time-dependent algorithms at very low Mach numbers should enhance our understanding at high Mach numbers as well. Finally, it is noted that the preconditioning scheme developed in Ref. 7 becomes ineffective when real gas properties (variable specific heats) are used as is often required in high-temperature problems. Consequently, a more detailed study of the low-Mach-number problem appears warranted.

The approach taken here is to use a perturbation expansion of the Euler equations in terms of Mach number squared[8,9] to develop an algorithm that will converge rapidly at arbitrarily low Mach numbers. The result gives an approximate set of equations that is valid at low Mach numbers, but which possesses well-conditioned eigenvalues that result in rapid convergence independent of the Mach number. Cases for Mach number 10^{-1} and 10^{-5} have shown identical rates of convergence, and there is no reason to expect this convergence rate to change until the Mach number becomes so small that machine underflows are encountered. It has been recently called to the authors' attention that a similar expansion scheme for low-Mach-number flows is being developed by Guerra and Gustafsson.[10] Instead of Mach number squared, their expansion is based on the first power of the Mach number.

The general nature of the expansion procedure in physical terms is to remove the rapidly propagating acoustic waves from the equation system and to replace them by a new set of "pseudo"-acoustic waves that travel at a "sound" speed that is the same order of magnitude as the flow velocity. The physical acoustic waves are removed by a formal perturbation expansion. The artificial acoustic waves are introduced by a proper selection of the time derivatives. These artificial acoustic waves then become the agents that propagate errors out of the flowfield and drive the solution to a steady state. The resulting procedure lacks the universality of the preconditioning schemes of Refs. 6 and 7 (most specifically, it is not valid at transonic speeds), but it is effective to much lower Mach numbers. An alternative procedure was proposed by Ramshaw et al.[11] who used a pressure gradient scaling in the momentum equation to reduce the effective acoustic speed. Their procedure, however, results in a modification of the steady-state equations whereas the present one does not.

Received Feb. 20, 1986; revision received Oct. 20, 1986.

*Professor, Department of Mechanical Engineering.
†Ph.D. Candidate, Department of Mechanical Engineering.

Problem Formulation

Development of the Low-Mach-Number Equations

The conservative form of the compressible Euler equations in two-dimensional, generalized coordinates is

$$\frac{\partial Q}{\partial t}+\frac{\partial E}{\partial \xi}+\frac{\partial F}{\partial \eta}=H \tag{1}$$

where the vectors Q, E, and F have their standard form

$$Q=J^{-1}(\rho,\ \rho u,\ \rho v,\ e)^T \tag{2a}$$

$$E=J^{-1}[\rho U,\ \rho Uu+\xi_x p,\ \rho Uv+\xi_y p,\ (e+p)U]^T \tag{2b}$$

$$F=J^{-1}[\rho V,\ \rho Vu+\eta_x p,\ \rho Vv+\eta_y P,\ (e+p)V]^T \tag{2c}$$

and the source term H contains both a volumetric heat addition rate and a gravitational body force,

$$H=J^{-1}(0,\ -\rho g,\ 0,\ q-\rho g u)^T \tag{2d}$$

In Eqs. (2), ρ and p represent the density and pressure; u and v are the velocity components in the Cartesian coordinates x and y; U and V are the contravariant velocity components in the transformed coordinates, ξ and η; J is the Jacobian of the transformation; and $e=\rho\epsilon+\frac{1}{2}\rho(u^2+v^2)$ is the total internal energy with ϵ being the thermodynamic internal energy. The Cartesian coordinates are chosen such that gravitational acceleration g is in the negative x direction. Heat is added to the flow by specifying the form of the volumetric heat addition function q. The gravitational term $\rho g u$ in the fourth component of H is the work done by the buoyancy force. This is small in most applications with buoyancy, and is ignored in the remainder of the paper.

To understand the behavior of the compressible equations as the Mach number is reduced, we first nondimensionalize all quantities in Eq. (1) by appropriate reference values. In so doing, we choose four independent reference quantities and relate all other properties to these basic four. We choose a reference velocity and a reference length u_r and L, along with the thermodynamic reference quantities ρ_r and T_r (T is the temperature). From the latter two, we define the reference pressure $p_r=\rho_r RT_r$ by using the perfect gas law. The reference total energy is also related to these two quantities as $e_r=\rho_r C_v T_r=\rho_r RT_r/(\gamma\text{-}1)$. (Here, C_v is the specific heat.) Finally, we use the reference velocity to define a reference Mach number, M_r, as $\gamma M_r^2=u_r^2/RT_r$, where γ is the ratio of specific heats.

With these nondimensionalizations, the perfect gas relation and the total energy become

$$\bar{p}=\bar{\rho}\bar{T}$$

$$\bar{e}=\bar{p}+\frac{\gamma-1}{2}\gamma M_r^2\bar{\rho}(\bar{u}^2+\bar{v}^2) \tag{3}$$

where overbars refer to nondimensional quantities. Another important outcome of the nondimensionalization is the form of the ρu^2+p terms that appear in the momentum equations. The nondimensionalization given above transforms terms of this type to the form $\bar{\rho}\bar{u}^2+\bar{p}/\gamma M_r^2$.

The low-Mach-number equations are obtained by expanding the nondimensional versions of Eqs. (2) in power series in the small parameter $\epsilon=\gamma M_r^2$ as

$$\bar{p}=p_0+\epsilon p_1+\ldots$$

$$\bar{u}=u_0+\epsilon u_1+\ldots \quad \text{etc.} \tag{4}$$

Upon substituting expansions of this form into Eq. (1) and collecting terms of like powers of ϵ, we obtain a sequence of equations, each of which must be satisfied independently. Because of the form of the ρu^2+p terms mentioned above, the power sequence in ϵ starts with $1/\epsilon$. For this order of approximation (ϵ^{-1}), we find

$$\frac{\partial}{\partial \xi}\left(\frac{\xi_x p_0}{J}\right)+\frac{\partial}{\partial \eta}\left(\frac{\eta_x p_0}{J}\right)=0$$

$$\frac{\partial}{\partial \xi}\left(\frac{\xi_y p_0}{J}\right)+\frac{\partial}{\partial \eta}\left(\frac{\eta_y p_0}{J}\right)=0 \tag{5}$$

which for orthogonal coordinates reduces to grad $p_0=0$. This equation states that the zero-order pressure is a function of time only. Because we are interested in steady-state solutions, we take p_0 as a constant. This result is analogous to classical approximations in combustion[12] that pressure is constant across a flame.

To order unity (ϵ^0), the equations become:

$$\frac{\partial Q_0}{\partial t}+\frac{\partial E_0}{\partial \xi}+\frac{\partial F_0}{\partial \eta}=H_0 \tag{6}$$

where the vectors, Q_0, E_0, and F_0, are

$$Q_0=J^{-1}[(\rho_0,(\rho u)_0,(\rho v)_0,p_0)]^T$$

$$E_0=J^{-1}[(\rho U)_0,\ (\rho Uu)_0+\xi_x p_1,(\rho Uv)_0+\xi_y p_1,\ \gamma p_0 U_0]^T$$

$$F_0=J^{-1}[(\rho V)_0,\ (\rho Vu)_0+\eta_x p_1,(\rho Vv)_0+\eta_y p_1,\gamma p_0 V_0]^T$$

$$H_0=J^{-1}(0,-\rho_0 g,\ 0,\ q_0)^T \tag{7}$$

This set of equations contains the four zero-order variables ρ_0, u_0, v_0, and p_0, but in addition, it also contains the first-order pressure, p_1. Since p_0 is determined from Eq. (5), the system of equations given by Eq. (6) represents four equations for the four variables ρ_0, u_0, v_0, and p_1. A major difficulty with Eq. (6) is that p_1 does not appear in the dependent variable Q_0. Because of this, it is impossible to express the vectors E_0 and F_0 as functions of Q_0 alone. Further, when p_0 is taken as a constant, the time derivative in the energy equation vanishes. Thus, the system given in Eq. (6) is analogous to the unsteady incompressible equations in that only three of the equations contain time derivatives while the fourth (in this case, the energy equation) does not.

To obtain a rapidly convergent time-iterative procedure for these low-Mach-number equations, we artificially add the time derivative of the missing variable, p_1, to the energy equation. This procedure is analogous to the one originally suggested by Chorin[13] for the incompressible equations that has been used with considerable success recently.[7,14,15] In adding this time derivative, we replace the vector Q_0 in Eq. (6) by the alternative vector Q_0', where,

$$Q_0'=J^{-1}[\rho_0,\ (\rho u)_0,\ (\rho v)_0,\ p_1/\beta]^T \tag{8}$$

This choice allows us to express $E_0=E(Q_0')$ and $F_0=F(Q_0')$, where these are unique functions. The parameter β is included to allow time scaling in the energy equation.

Numerical Solution Procedure

Accurate steady-state solutions of the low-Mach-number equations

$$\frac{\partial Q_0'}{\partial t}+\frac{\partial E_0}{\partial \xi}+\frac{\partial F_0}{\partial \eta}=H_0 \tag{9}$$

given above can now proceed by standard time-iterative schemes of either an explicit or implicit variety. In the present paper, an Euler-implicit[16,17] scheme has been chosen,

although explicit schemes[18,19] have also been considered as is discussed later.

In any numerical scheme, the Jacobians of the vectors E_0, F_0, and H_0 play a key role (even though they may not appear directly in some explicit schemes), but because their computation is straightforward, their form will be omitted here. The main impact of these Jacobian matrices can be ascertained from their eigenvalues. For the matrix $A = \partial E_0/\partial Q_0'$, the eigenvalues are

$$\lambda(A) = \left(\overline{U}_0, \overline{U}_0, \frac{\overline{U}_0 + \bar{c}'}{2}, \frac{\overline{U}_0 - \bar{c}'}{2}\right) \tag{10}$$

where

$$\bar{c}' = [\bar{U}_0^2 + 4\beta\gamma\bar{p}_0/\bar{\rho}_0(\xi_x^2 + \xi_y^2)]^{1/2} \tag{11a}$$

Because all quantities appearing in Eq. (11a) are nondimensional, we see that c' will be of order U_0 providing we choose β to scale out the effect of the transformation. Thus, choosing $\beta = \frac{1}{4}\gamma$, we have

$$\bar{c}' = [\overline{U}_0^2 + \bar{p}_0/\bar{\rho}_0(\xi_x^2 + \xi_y^2)]^{1/2} \tag{11b}$$

In dimensional form, we have

$$c' = [U_0^2 + c_0^2(\xi_x^2 + \xi_y^2)]^{1/2} \tag{11c}$$

The low-Mach-number expansion procedure is thus seen to have removed the physical acoustic speed c, which is large compared with the velocity u ($c \gg u$). Adding the artificial time derivative to the energy equation has in its place introduced a pseudoacoustic speed c' whose speed is of the same order as the particle velocity u as is shown by Eq. (11c). Similar analysis gives analogous conclusions for the flux vector F_0.

Applying Euler implicit differencing in time and three-point central differencing in space yields the approximately factored algorithm in delta form[16,17]

$$(P + \Delta t\delta_\xi A)P^{-1}\ (P + \Delta t\delta_\eta B)\Delta Q = -\Delta t(\delta_\xi E_0 + \delta_\eta F_0 - H_0)^n \tag{12}$$

where

$$P = I - D\Delta t \tag{13}$$

Here, δ represents the central difference operator, $\Delta Q = Q_0'^{n+1} - Q_0'^n$, and the superscript n refers to the time step. The matrices B and D are the Jacobians $B = \partial F_0/\partial Q_0'$ and $D = \partial H_0/\partial Q_0'$. The solution of Eq. (12) requires standard block tridiagonal matrix procedures. In some calculations, a small amount of fourth order viscosity[7,20] was added, but it was treated in an explicit manner.

Boundary Conditions

The proper choice of boundary conditions is extremely important to any algorithm. For the present system of equations, the pseudoacoustic waves ensure that three eigenvalues are always positive (for $U > 0$) while one is negative ("subsonic" flow). This means we must specify three boundary conditions at the upstream end and one at the downstream end. The remaining conditions that determine ΔQ on the upstream and downstream boundaries (four conditions are needed) must come from the equations of motion. This information is extracted from the modified low-Mach-number system using the method of characteristics in an implicit fashion.

For all cases, the single-boundary condition imposed at the downstream end was the specification of a constant static pressure. At the upstream end, the stagnation temperature and the flow angle V/U were fixed. Two different conditions corresponding to two different physical situations were used for the third upstream boundary condition. In one, the upstream stagnation pressure was fixed to simulate flow from a plenum. For this condition, the downstream exit pressure determines the mass flow. In the second type of calculation, the upstream velocity U was specified as a given function of the cross-stream direction (generally a constant). This corresponds to an internal flow system that is being fed from an (upstream) choked orifice that sets the mass flow. In this case, the downstream pressure fixes the pressure level in the system.

Along the nozzle wall, the contravariant velocity V is set to zero to ensure flow tangency, and the method of characteristics is again used to complete the specification of ΔQ on the boundary. At the centerline, symmetry conditions are used in lieu of a boundary condition so the axis of symmetry is treated as a regular field point.

The boundary condition information on all boundaries was augmented by information form the equations of motion by using the method of characteristics procedure suggested by Chakravarthy[21] and Rai and Chaussee[22] as implemented in Refs. 4 and 7. In this procedure, we premultiply Eq. (12) by the modal matrix containing the left eigenvectors of the Jacobian A (or B) for a ξ (or η) boundary and then multiply this result by a selection matrix that selects those characteristic equations that represent information propagating toward the boundaries. This reduced set of equations is then combined with the boundary conditions to give four equations for the four unknowns, ΔQ, on the boundaries. In evaluating derivatives normal to the boundary in these expressions, three-point one-sided relations are used. As always, the use of first- or second-order accurate derivatives at the boundaries has little effect on the rate of convergence, but three-point differences typically reduce any odd-even oscillations in the converged solution by almost an order of magnitude.

Results

Stability Analysis of the Low-Mach-Number System

Prior to attempting numerical solutions of a new system of equations, it is useful to assess the stability characteristics of the discretized equations. By treating the coefficient matrices in Eq. (12) as locally constant, we can apply Fourier transform methods to the complete low-Mach-number equations. Although such analyses can only be expected to be qualitatively accurate, they represent nearly the only way to obtain fundamental understanding of the complete discretized equation system. Such an analysis cannot replace numerical experimentation, but it can provide much-needed understanding and guidance.

Applying an Euler-implicit, central-difference scheme to Eq. (9) and using a Douglas-Gunn[23] consistent splitting results in the discretized scheme given in Eq. (12). Performing a Fourier transform of the locally linearized version of Eq. (12) yields an amplification matrix G that is given by

$$G = K_1^{-1}K_2 \tag{14}$$

where

$$K_1 = I - \Delta t^2 AP^{-1}B\, S_\xi S_\eta - \omega_e/2[(1 - C_\xi)^2 + (1 - C_\eta)^2]I \tag{15a}$$

$$K_2 = P + i\Delta t(AS_\xi + BS_\eta) - \Delta t^2 AP^{-1}BS_\xi S_\eta \tag{15b}$$

Here, S and C represent the sine and cosine, respectively, of the Fourier modes in the ξ or η direction (as indicated by subscript). The quantity ω_e represents an explicit, fourth-order artificial viscosity that is included for generality.

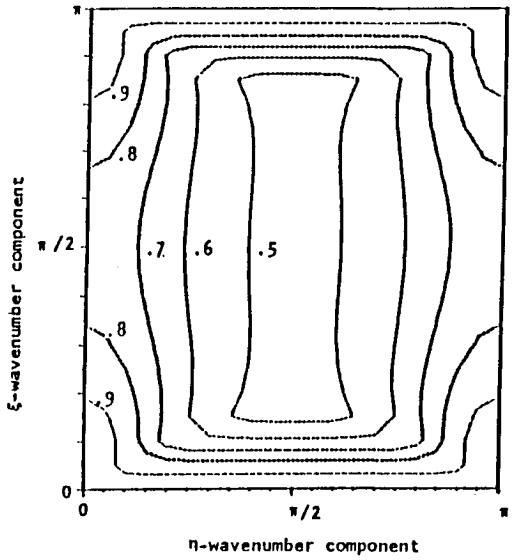

Fig. 1 Contour plot of maximum eigenvalues in vector stability calculation for low-Mach-number equations without buoyancy and without approximate factorization; $M_x = 10^{-3}$, $M_y = 0$, $\omega_e = 0$, $CFL = 5$.

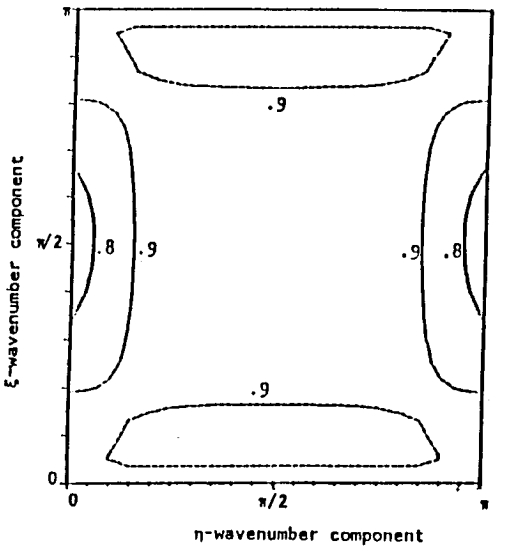

Fig. 2 Contour plot of maximum eigenvalues from vector stability calculations for low-Mach-number equations without buoyancy, but with approximate factorization; $M_x = 10^{-3}$, $M_y = 0$, $\omega_e = 0$, $CFL = 5$.

The eigenvalues of the 4×4 matrix G determine the stability of the numerical algorithm. By computing these eigenvalues numerically, we can study the effect of various parameters on solution convergence. Representative calculations for four different conditions are summarized in Figs. 1-4. For brevity, only the largest of the four eigenvalues has been presented in each case. Figures 1 and 2 show the effect of approximate factorization in the absence of buoyancy. Figure 1 is for the exact Euler-implicit algorithm [the Δt^2 terms in Eq. (12) and (15) have been dropped], while Fig. 2 shows corresponding results for the case where approximate factorization is included. In the absence of approximate factorization (Fig. 1), the eigenvalues are near unity around the periphery of the wavenumber domain and drop toward a relative minimum in the central portion where the amplification factor falls below 0.5. When approximate factorization is included (Fig. 2), the central portion of wavenumber space becomes a relative maximum and takes on values that are larger than 0.9. The differences between these two plots show the strong detrimental effect of approximate factorization, an effect that grows ever larger as CFL is increased. The eigenvalues remain unconditionally stable in the presence of approximate factorization, but their magnitudes approach unity throughout the entire wavenumber domain thus substantially slowing the convergence of the numerical algorithm. The value of CFL used throughout is based on the maximum eigenvalue in Eq. (10) as $CFL = \lambda_{\max} \Delta t / \Delta \xi$.

Figures 3 and 4 show a similar comparison of the effect of approximate factorization when buoyancy is included. Without approximate factorization, the effect of the source term due to buoyancy is to add small unstable regions near the four corners of the wavenumber domain (compare with Fig. 1). These small unstable regions can be removed easily by a small amount of fourth order viscosity (ω_e is taken as zero in all four figures), and do not pose much of a problem. What is more troublesome is the manner in which these unstable regions grow when approximate factorization is used. Figure 4 shows that, in this case, the unstable regions extend across the wavenumber spectrum. This extended unstable region can no longer be neutralized by reasonable amounts of fourth order viscosity and an alternative procedure is required. Additional stability calculations at other Mach numbers (Fig. 4 is for a Mach number of 10^{-3}) indicate that the unstable region disappears entirely at Mach numbers slightly higher than this value, but that the unstable area gets rapidly larger and the magnitudes of the unstable eigenvalues grow as the Mach number is reduced. Proper nondimensionalization of the equations shows that it is the Froude number, $F_r = u_{\text{in}}^2 / gL$, not the Mach number that controls stability. For the present case, the Froude number was 0.42. Because we are physically more interested in the flow Mach number, we will quote both quantities hereafter. Because of this instability, we anticipate convergence difficulties when the flow velocities get small enough that buoyancy begins to dominate.

Fortunately, our primary interests are above this Mach number and the present algorithm is sufficient for many cases of interest. A discussion of methods for avoiding the instabilities caused by this buoyancy induced source term is given in Ref. 24.

Heat Addition in a Constant Area Duct

As an initial demonstration of the low-Mach-number formulation, we consider the upward flow of gas through a constant area duct with specified heat addition. In these calculations, the heat addition per unit volume rather than per unit mass is specified so the peak temperature of the gas is inversely proportional to the velocity. The heat source is defined in terms of the algebraic function $F(x,y)$ as

$$q = P \text{ Min } \{ [2F^{3/2} - 3F + 1], 1 \} \tag{16}$$

where

$$F(x,y) = \frac{(x - x_a)^2 + (y - y_a)^2}{(x_b - x_a)^2 + (y_b - y_a)^2} \tag{17}$$

and where P is a scaling variable. This gives a circular zone of heat addition with a maximum heating rate P at the center that decays smoothly to zero on the circle where F approaches one. For the calculations presented here, the heating zone was centered in the middle of the flow duct with the parameter values (normalized by the duct length) $x_a = 0.125$, $x_b = 0.065$, $y_a = y_b = 0.1$. The duct itself was taken as unit length (0.25 m) with a full width of 0.2. Although the computer code used was written in fully transformed generalized coordinates, some of the present calculations were performed on an unstretched grid. Calculations with and without the effects of gravity are shown in Figs. 5-11.

Figure 5 shows the converged temperature contours for an inlet Mach number of 0.01 ($F_r = 50$). The left-hand half of

the figure neglects the effects of gravity, the right-hand half includes gravity. This velocity is high enough to eliminate gravitational effects: the two halves of the figure are nearly identical. Figure 6 shows the companion velocity contours for these two calculations. Again, gravity has a negligible effect. The heating accelerates the flow near the upper (outlet), central portion of the channel, but at the inlet, the heat addition acts as a blockage that slows down the incoming flow. (Inlet boundary conditions here correspond to those of a reservoir.) The heating rates for this case produce a temperature change T_{max}/T_{in} of more than six.

Corresponding calculations for an inlet Mach number of 1.5×10^{-3} ($F_r=0.95$) are given in Figs. 7 and 8. As noted above, this condition is marginal with respect to convergence. The calculations in the presence of gravity lead to a lower peak temperature because the buoyant acceleration moves the gas through the heating zone more rapidly. For otherwise similar conditions, the flow without gravity has a maximum temperature change T_{max}/T_{in} of 6.33, while in the presence of gravity the peak temperature is 4.67. Analogous differences are observed in the velocity as shown in Fig. 8. In the absence of gravity, the flow decelerates after it reaches the peak heating point. In the presence of gravity, it accelerates after the peak heating rate because of the buoyant acceleration.

The rate of convergence of solutions at this inlet Mach number is shown in Fig. 9. The rate of convergence without buoyancy is good, but the convergence with buoyancy has started to slow down. Further decreases in inlet Mach number (Froude number) cause the convergence rate for the case with gravity to decrease gradually until divergence occurs. The calculations without gravity continue to converge at the same rate as that shown in Fig. 9 down to at least a Mach number of 10^{-5}.

To demonstrate convergence at lower Mach numbers in the absence of gravity, Fig. 10 shows both the temperature contours (right half) and the velocity contours (left half) for

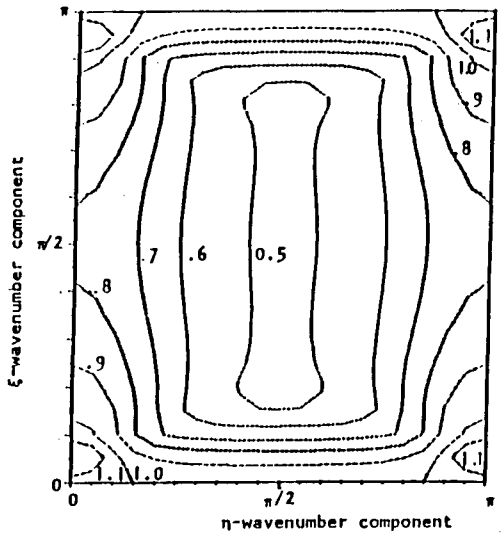

Fig. 3 Contour plot of maximum eigenvalues for vector stability analysis of low-Mach-number equations with buoyancy, but without approximate factorization; $M_x=10^{-3}$, $M_y=0$, $F_r=0.42$, $\omega_e=0$, $CFL=5$.

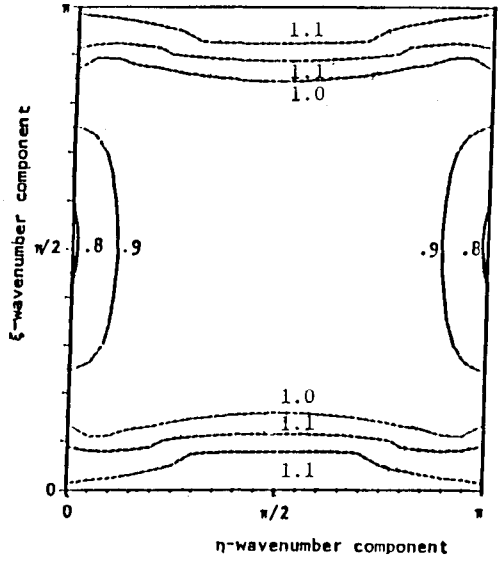

Fig. 4 Contour plot for maximum eigenvalues from vector stability analysis of low-Mach-number equations with buoyancy. Results include effects of approximate factorization; $M_x=10^{-3}$, $M_y=0$, $F_r=0.42$, $\omega_e=0$, $CFL=5$.

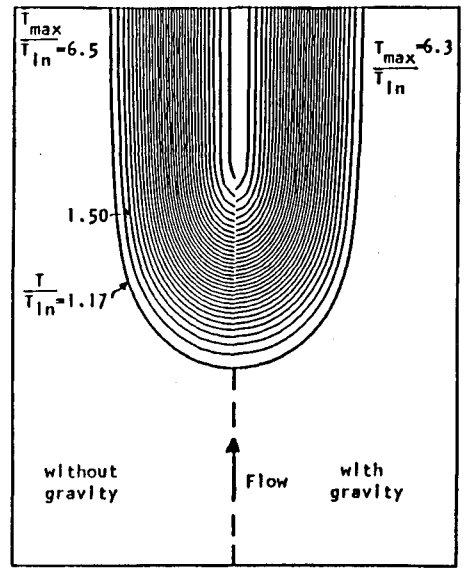

Fig. 5 Temperature contours for volumetric heating of a gas; inlet Mach number 10^{-2}, $F_r=50$, $P=8\times10^7$ w/m^3/m. Left-hand side is without gravity; right-hand side is with gravity; $\omega_e=0$, $CFL=5$.

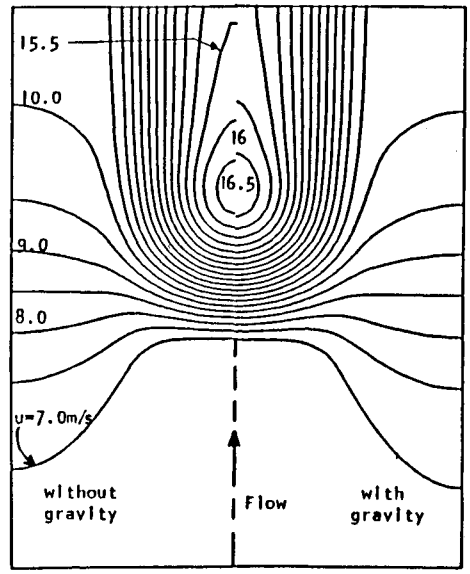

Fig. 6 Velocity contours for volumetric heating of a gas; inlet Mach number 10^{-2}, $F_r=50$, $P=8\times10^7$ w/m^2/m. Left-hand side is without gravity; right-hand side is with gravity; $\omega_e=0$, $CFL=5$.

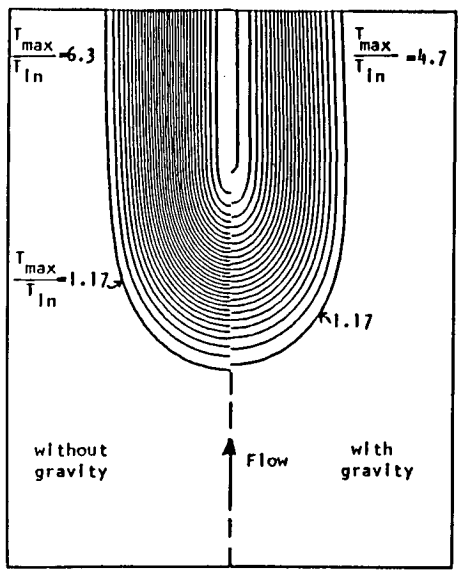

Fig. 7 Temperature contours for volumetric heating in a duct; inlet Mach number 1.5×10^{-3}, $F_r=0.95$, $P=1.2\times10^7$ w/m^2/m. Left-hand side is without gravity; right-hand side is with gravity; $\omega_e=0.25$, $CFL=5$.

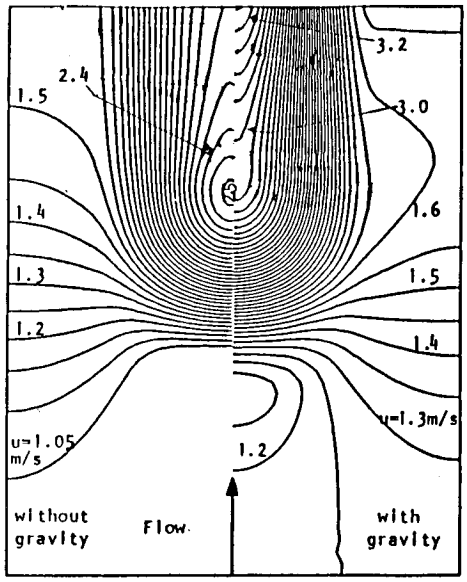

Fig. 8 Velocity contours for volumetric heating in a duct; inlet Mach number 1.5×10^{-3}, $F_r=0.95$, $P=1.2\times10^7$, w/m^2/m. Left-hand side is without gravity; right-hand side is with gravity; $\omega_e=0.25$, $CFL=5$.

a flow with an inlet Mach number of 1×10^{-5}. Convergence for this case is identical to the "without gravity" case in Fig. 9. The corresponding case including gravity failed to converge.

All cases presented thus far are for constant stagnation pressure conditions at the upstream boundary simulating flow drawn from a large reservoir. To test sensitivity to boundary conditions, the u-velocity at the upstream boundary was specified and a case analogous to that in Fig. 8 was computed. Specifying the velocity (mass flow) at the upstream end is analogous to adding heat in a duct in which the mass flow is fixed at some upstream location by a choked orifice. The results look qualitatively the same as shown by the temperature/velocity contour plot in Fig. 11, but the blockage effect of the heating that causes nonuniform velocities at the inlet plane for the reservoir calculations is now removed. The convergence rate for this case was again identical to that given in Fig. 9.

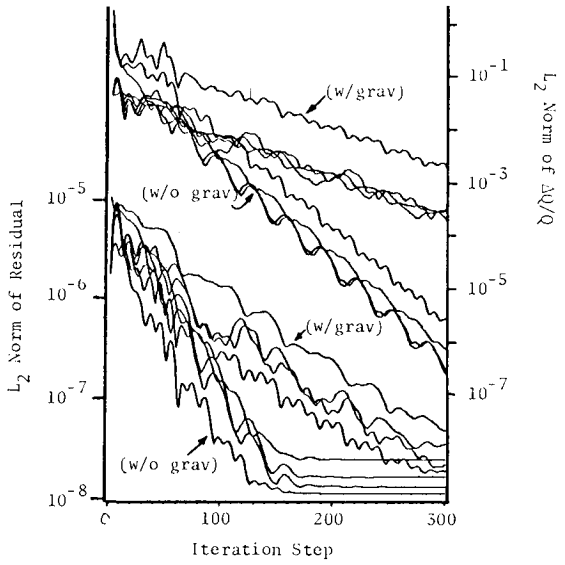

Fig. 9 Rate of convergence of calculations at an inlet Mach number of 1.5×10^{-3}, $F_r=0.95$, in terms of L_2 norms.

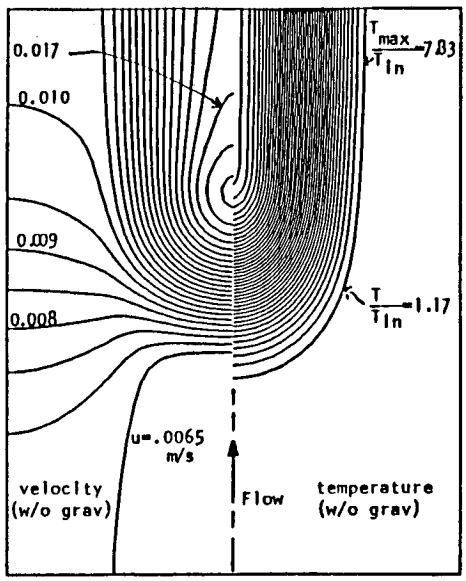

Fig. 10 Velocity (left side) and temperature (right side) contours for an inlet Mach number of 10^{-5}. $P=9\times10^4$ w/m^2/m. Without gravity; $\omega_e=0$, $CFL=5$.

Laser Heat Addition in a Constant Absorptivity Gas

As a second problem, we consider heat addition in a constant absorptivity gas by an incoming laser beam.[2,4] A schematic picture of the laser beam is given in Fig. 12. For this constant absorptivity case the laser problem also represents a specified heat addition calculation, but the heating pattern is very different than in the previous case. To resolve the much narrower heating region, a stretched grid has been used as shown in Fig. 12. Representative results for this case are given in Figs. 13 and 14. Figure 13 is for a temperature rise T_{max}/T_{in} of 3.6 and a Mach number of 2×10^{-3}. Figure 14 is for a temperature rise of 5.6 and a Mach number of 1.5×10^{-5}. Both of these results are for the no-gravity case.

A summary plot of laser absorption calculations is given in Fig. 15. This figure shows the maximum temperature as a function of the inlet velocity for both the buoyant and the nonbuoyant cases. Results are shown for laser beams with the same focal length (the same distribution of heat addition) but for different laser powers (different overall heat addition

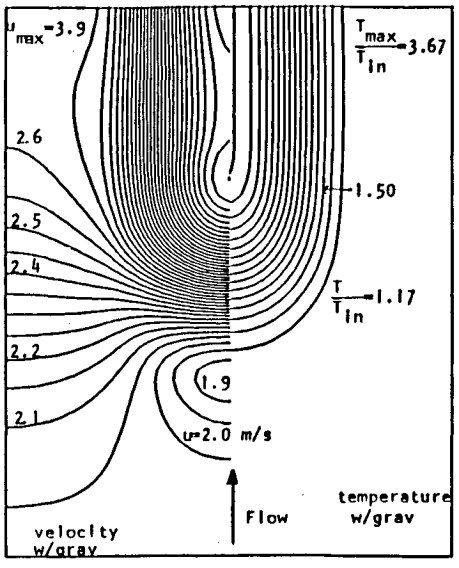

Fig. 11 Temperature and velocity contours for specified mass flow case; inlet Mach number 2×10^{-3}, $F_r=1.7$. With gravity; $\omega_e=0.25$, $CFL=5$.

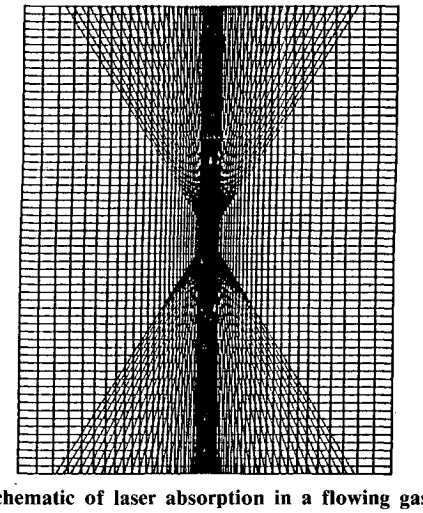

Fig. 12 Schematic of laser absorption in a flowing gas. Diagonal lines outline focused laser beam and show manner in which beam is discretized. Both the flow and the converging beam go from bottom to top.

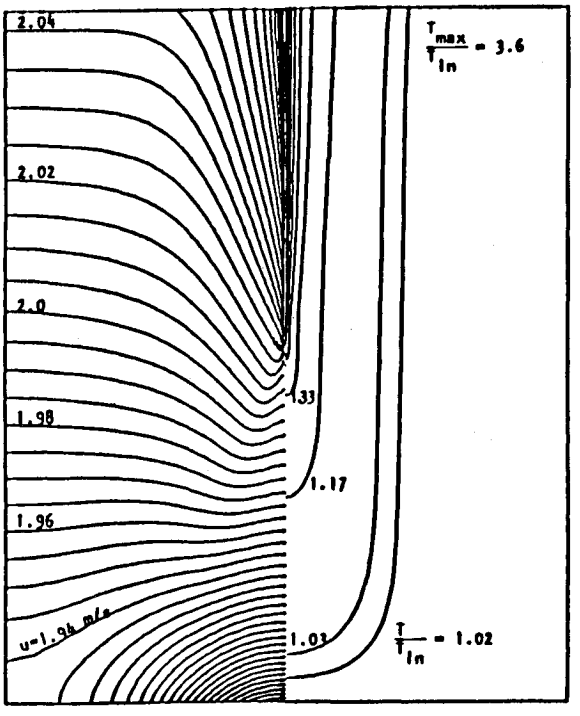

Fig. 13 Temperature and velocity contours in laser absorption problem. Inlet Mach number 2×10^{-3}; laser power 5×10^{3} w/m, without gravity. Flow is from bottom to top; $\omega_e=0.25$, $CFL=5$.

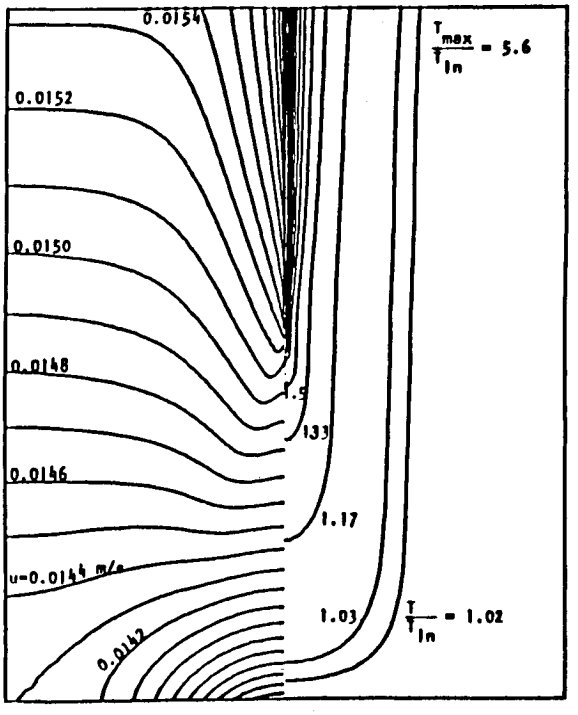

Fig. 14 Temperature contours in laser absorption problem. Inlet Mach number 1.5×10^{-5}; laser power 80 w/m, without gravity. Flow is from bottom to top; $\omega_e=0.25$, $CFL=5$.

rates). Again, the low-Mach-number formulation converged reliably at all Mach numbers in the absence of gravity. When gravity is present, calculations could only be obtained for inlet Mach numbers above 10^{-3} (and for Froude numbers above 1). This stability limit is independent of the heating rate and also exists when there is no heating at all. This observation directly corroborates stability predictions. The results do, however, extend low enough to show the manner in which buoyancy begins to dominate at very low velocities.

Summary

A method for computing compressible flows at low Mach numbers has been developed and tested. The method is based on a perturbation expansion of the Euler equations in terms of the Mach number. The equation system that is obtained shows that the pressure is constant to first order, in agreement with a commonly invoked assumption in combustion. In physical terms, the perturbation expansion removes the rapidly propagating acoustic disturbances from the unsteady equation system. The resulting system is no longer hyperbolic in time because the energy equation becomes a steady compatibility condition without a time derivative. To make the perturbed system hyperbolic, we add a time derivative (of the perturbation pressure) to the energy equation. This artificial time derivative renders the equations invalid in unsteady conditions, but does provide an effective time-iterative path for obtaining steady solutions. With this artificial time derivative added, the equations possess an artificial acoustic speed that is of the same order of magnitude as the particle velocity. These artificial acoustic waves are effective in propagating errors out of the flowfield, and the

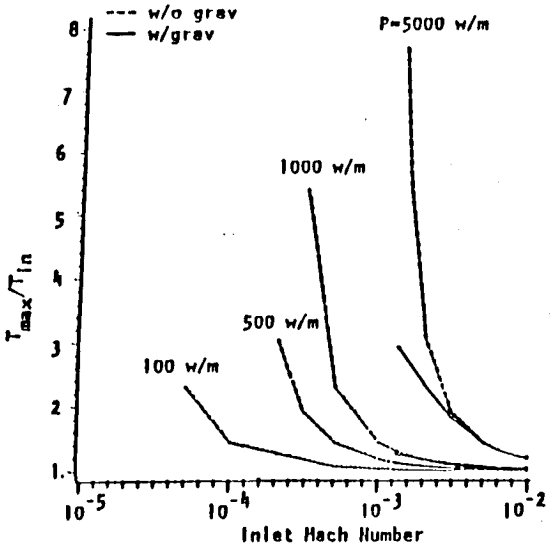

Fig. 15 Peak temperature as a function of inlet Mach number for various laser power laser levels comparing calculations with and without gravity.

scheme is uniformly successful in providing efficient computations at arbitrarily low Mach numbers.

By formulating these low-Mach-number equations in the standard vector form, we can use classical time-iterative procedures including approximate factorization of an algorithm in delta form to obtain its numerical solution. Through the use of formal vector manipulations based upon the method of characteristics, the boundary conditions can likewise be applied in a standard manner. The equations used at the boundaries are much different than for compressible flows, but the procedures are analogous. The overall result is that although a compressible code must be modified to accommodate this low-Mach-number formulation, its overall structure remains unchanged.

Results computed for flow through a duct with substantial heat addition have shown convergence rates that are independent of flow Mach number to as low as 10^{-5}. The convergence rate is similar to that obtained with compressible codes at high subsonic Mach numbers, as well as with incompressible codes based on artificial compressibility. The use of a common algorithm and analogous boundary conditions for three distinct sets of conservation laws demonstrates the wide applicability of the time-iterative technique.

Low-Mach-number flowfields with heat addition raise the possibility that buoyancy may be significant, and its effect has likewise been addressed. Buoyancy forces appear as a source term in the equations of motion. Their effect is somewhat different from other source terms. Stability results suggests instabilities will be encountered when the Froude number is less than 1.0. Computational experiments confirm this; when gravity is included, the present scheme will not converge below a Mach number of 10^{-3} ($F_r = 0.42$). A modification of this procedure that does allow strongly buoyant flows to be computed is presented in Ref. 24.

Acknowledgment

This work was sponsored by the Air Force Office of Scientific Research under Contract AFOSR 82-0196.

References

[1]Kemp, N. H. and Root, R. G., "Analytical Study of Laser-Supported Combustion Waves in Hydrogen," *Journal of Energy*, Vol. 3, Jan.-Feb. 1979, pp. 40-49.

[2]Keefer, D., Welle, R, and Peters, C., "Power Absorption Processes in Laser-Sustained Argon Plasmas," AIAA Paper 85-1552, July 1985.

[3]Merkle, C. L., "Prediction of the Flowfield in Laser Propulsion Devices," *AIAA Journal*, Vol. 22, Aug. 1984, pp. 1101-1107.

[4]Molvik, G. A., Choi, D., and Merkle, C. L., "A Two-Dimensional Analysis of Laser Heat Addition in a Constant Absorptivity Gas," *AIAA Journal*, Vol. 23, July 1985, pp. 1053-1060.

[5]Briley, W. R., McDonald, H., and Shamroth, S. J., "A Low Mach Number Euler Formulation and Application to Time-Iterative LBI Schemes," *AIAA Journal*, Vol. 21, Oct. 1983, pp. 1467-1469.

[6]Turkel, E., "Fast Solutions to the Steady State Compressible and Incompressible Fluid Dynamic Equations," ICASE Rept. 84-28, NASA C-172416, June 1984.

[7]Merkle, C. L. and Choi, D., "Application of Time-Iterative Schemes to Incompressible Flow," *AIAA Journal*, Vol. 23, Oct. 1985, pp. 1518-1524.

[8]Rehm, R. G. and Baum, H. R., "The Equations of Motion for Thermally Driven, Buoyant Flows," *Journal of Research of the National Bureau of Standards*, Vol. 83, No. 3, May-June 1978, pp. 297-308.

[9]Oran, E. S. and Boris, J. P., "Detailed Modelling of Combustion Systems," *Progress in Energy and Combustion Science*, Vol. 7, 1981, pp. 1-72.

[10]Guerra, J. and Gustafsson, B., "Numerical Method for Incompressible and Compressible Flow Problems with Smooth Solutions," *Journal Computational Physics*, Vol. 63, April 1986, pp. 377-397.

[11]Ramshaw, J. D., O'Rourke, P. J., and Stein, L. R., "Pressure Gradient Scaling Method for Fluid Flow with Nearly Uniform Pressure," *Journal of Computational Physics*, Vol. 58, May 1985, pp. 361-376.

[12]Williams, F. A., *Combustion Theory, The Fundamental Theory of Chemically Reacting Flow Systems*, Addison-Wesley, Reading, MA, 1965.

[13]Chorin, A. J., "A Numerical Method for Solving Incompressible Viscous Flow Problems," *Journal of Computational Physics*, Vol. 2, Aug. 1967, pp. 12-26.

[14]Chang, J.L.C. and Kwak, D., "On the Method of Pseudo-Compressibility for Numerically Solving Incompressible Flows," AIAA Paper 84-0252, Jan. 1984.

[15]Kwak, D., Chang, J.L.C., and Chakravarthy, S. R., "An Incompressible Navier-Stokes Flow Solver in Three-Dimensional Curvilinear Coordinate System Using Primitive Variables," AIAA Paper 84-0253, Jan. 1984.

[16]Briley, W. R. and McDonald, H., "On the Structure and Use of Linearized Block Implicit Schemes," *Journal of Computational Physics*, Vol. 34, Jan. 1980, pp. 54-73.

[17]Warming, R. F. and Beam, R. M., "On the Construction and Application of Implicit Factored Schemes for Conservation Laws," *SIAM-AMS Proceedings*, Vol. 11, 1978, pp. 85-129.

[18]Jameson, A., Schmidt, W., and Turkel, E., "Numerical Solutions of the Euler Equations by Finite Volume Methods Using Runge-Kutta Time-Stepping Schemes," AIAA Paper 81-1259, June 1981.

[19]Jameson, A. and Baker, T. J., "Solution of the Euler Equations for Complex Configurations," AIAA Paper 83-1929, July 1983.

[20]Steger, J. L., "Implicit Finite-Difference Simulation of Flow About Arbitrary Two-Dimensional Geometries," *AIAA Journal*, Vol. 16, July 1978, pp. 679-686.

[21]Chakravarthy, S. R., "Euler Equations—Implicit Schemes and Implicit Boundary Conditions," *AIAA Journal*, Vol. 21, May 1983, pp. 699-706.

[22]Rai, M.M. and Chaussee, D. S., "New Implicit Schemes and Implicit Boundary Conditions," AIAA Paper 83-0123, Jan. 1983.

[23]Douglas, J. and Gunn, J. E., "A General Formulation of Alternating Direction Methods, Part I, Parabolic and Hyperbolic Problems," *Numerische Mathematik*, Vol. 6, 1964, pp. 428-453.

[24]Merkle, C. L. and Choi, Y.-H., "Computation of Low Mach Number Flows With Buoyancy," presented at the 10th International Conference on Numerical Methods in Fluid Dynamics, Beijing, China, June 1986.